X-RAY SPECTROMETRY
X-Ray Spectrom. 2001; **30**: 127–131

XRS

Background spectrum of synchrotron radiation-excited total reflection x-ray fluorescence for Si wafer analysis

N. S. Shin,[1]* C. H. Chang,[2] Y. M. Koo[1] and H. Padmore[3]

[1]Pohang Accelerator Laboratory, Pohang 790-784, Republic of Korea
[2]Research Institute of Industrial Science and Technology, Pohang 790-600, Republic of Korea
[3]Lawrence Berkeley National Laboratory, Berkeley, California 94720, USA

Received 25 September 2000; Accepted 9 December 2000

In the synchrotron radiation-excited total reflection x-ray fluorescence (SR-TXRF) determination of surface contaminants on Si wafers, the minimum detection limit is intrinsically determined by the background spectrum. The absolute counts of background spectra for the whole energy range concerned was calculated under the usual SR-TXRF experimental conditions and was compared with measurements. The detection limits for contaminants near the surface of Si wafers within a few atomic layers were evaluated from the calculated background spectrum and the fluorescence signal under given experimental conditions.

INTRODUCTION

The total reflection x-ray fluorescence (TXRF) method has been widely used in the semiconductor industry to determine surface contaminants of Si wafers. The demand to detect surface contamination by transition metals in the order of 10^7 atoms cm^{-2} is rising rapidly as the structural dimensions of semiconductor devices continue to shrink. The minimum detection limit (MDL) in TXRF is usually evaluated by $3C_{std}\sqrt{N_B}/N_P$, where C_{std} is the concentration of a standard, N_B is the background counts and N_P is the net peak area. From this definition, it follows that lower MDLs in TXRF can be obtained by brighter excitation sources, a higher speed detection system and lower background spectrum intensity excitation. It is expected that TXRF using synchrotron radiation (SR-TXRF), owing to its high brightness and linear polarization, will satisfy the future demands.[1–5]

The calculation of the absolute background spectrum is of importance not only to determine the detection limits of contaminants but also to investigate the optimum SR-TXRF experimental conditions, such as the energy of incident x-rays, the glancing angle and the experimental arrangement of the wafer and detector system. So far, the theoretical evaluation of the background spectrum, the major determinant of the intrinsic MDL, has not been performed for the whole energy range of a TXRF spectrum. The calculation of a TXRF background spectrum in the lower energy range, which predominantly consists of bremsstrahlung emitted by photoelectrons, was presented in a previous paper.[6] The calculations of the background spectrum due to photoelectron bremsstrahlung indicated the presence of another source of background spectrum in the higher energy range of the contaminant elements Ni, Cu, Zn, etc. SR-TXRF measurements for the trace element analysis of Si wafers are usually carried out with an incident beam energy of about 11 keV. Under this condition, Ortega *et al.* regarded Compton scattering as the limiting factor for the determination of Cu and Zn.[2]

In this study, we evaluated the absolute counts of background spectra for the whole energy range under given experimental conditions for SR-TXRF measurements of Si wafer surfaces. The theoretical results were compared with measured spectra. Based on these results, the theoretical MDLs of surface contaminations achievable under certain experimental conditions were also evaluated.

CALCULATION OF COMPTON SCATTERED SPECTRUM

The influence of the SiO_2 layer formed on Si wafers is taken into account, because of the difference in Compton scattering cross-sections between Si and SiO_2 and the variation of the incident x-ray intensity distribution near the wafer surface. The Compton scattered spectrum striking the detector is obtained by integrating the Compton scattering cross-section over the detecting area and the effectively irradiated area of the Si wafer:

$$\frac{dI_{COMS}(E)}{dE} = 2A\int_0^{2\pi}\int_0^{R_{eff}}\int_0^{\phi_2}\int_{\theta_1}^{\theta_2}\left[\frac{\rho_{SiO_2}}{M_{SiO_2}}\sum_i\left(\frac{d^2\sigma_{SiO_2}}{d\Omega\,dE}\right)_i \times\int_0^d I(I_0,\alpha,d,z)\,dz + \frac{\rho_{Si}}{M_{Si}}\sum_j\left(\frac{d^2\sigma_{Si}}{d\Omega\,dE}\right)_j \times\int_d^\infty I(I_0,\alpha,d,z)\,dz\right]\sin\theta\,d\theta\,d\phi R\,dR\,d\Phi \quad (1)$$

where A is Avogadro's number, ρ the density, M the molecular weight and $(d^2\sigma/d\Omega\,dE)_i$ the Compton scattering cross-section of the ith shell. The subscripts SiO_2 and Si refer to the SiO_2 layer and Si wafer, respectively. $I(I_0,\alpha,d,z)$ is the x-ray intensity at depth z and α is the glancing angle. I_0

*Correspondence to: N. S. Shin, Pohang Accelerator Laboratory, Pohang 790-784, Republic of Korea.

and d are the incident x-ray intensity and the thickness of the SiO_2 layer on the Si wafer, respectively. The geometric parameters θ, ϕ, R and Φ are defined in Fig. 1. The integration limits of Eqn (1) over the detecting surface (radius R_s) and the effectively irradiated area of the Si wafer (radius R_{eff}) for the experimental conditions in Fig. 1 are given by

$$\phi_2 = \begin{cases} \sin^{-1}\left[\dfrac{R_s}{R}\left(\dfrac{R_{eff}^2 - R^2}{R_{eff}^2 - R_s^2}\right)^{1/2}\right] & \text{for } R \geq R_s \\ \pi & \text{for } R < R_s \end{cases}$$

$$\theta_1 = \begin{cases} \tan^{-1}\left[\dfrac{R\cos\phi - (R_s^2 - R^2\sin^2\phi)^{1/2}}{Z_g}\right] & \text{for } R \geq R_s \\ 0 & \text{for } R < R_s \end{cases}$$

$$\theta_2 = \tan^{-1}\left[\frac{R\cos\phi - (R_s^2 - R^2\sin^2\phi)^{1/2}}{Z_s}\right]$$

$$R_{eff} = R_s(Z_s + Z_g)/(Z_s - Z_g)$$

where Z_s and Z_g are the normal distances of the detector crystal and the collimator from the Si wafer surface, respectively.

For the double differential Compton scattering cross-section with respect to the scattering angle and scattered photon energy, Ribberfors' equation based on a relativistic impulse approximation is used.[7,8] In the geometry for the SR-TXRF measurement in this study, the electric field vector of the incident synchrotron radiation is assumed to be linearly polarized and the detector axis is normal and in the same plane for reducing the background counts. With the definitions in Fig. 1, the differential Compton scattering cross-section is expressed by

$$\left(\frac{d^2\sigma}{d\Omega\, dE}\right)_i = \frac{r_0^2}{2}\frac{E}{E_0}\frac{mc}{[E_0^2 + E^2 - 2E_0E\sin\theta\cos(\phi + \Phi)]^{1/2} - (E_0 - E)P_z/mc} \times \left[\frac{E_c}{E_0} + \frac{E_0}{E_c} - 2\cos^2\theta\right] J_i(P_z) \quad (2)$$

where

$$P_z = mc\frac{E - E_0 + E_0E[1 - \sin\theta\cos(\phi + \Phi)]/mc^2}{[E_0^2 + E^2 - 2E_0E\sin\theta\cos(\phi + \Phi)]^{1/2}}$$

$$E_c = \frac{E_0}{1 + E_0[1 - \sin\theta\cos(\phi + \Phi)]/mc^2}$$

and r_0, m and c are the classical electron radius, the mass of an electron at rest and the speed of light, respectively. E_0 and E are the incident and Compton scattered photon energy and E_c is the Compton scattered photon energy for an electron at rest. $J_i(P_z)$ is the Compton profile of an electron in the ith shell and P_z is the projection of the electron's pre-collision momentum on the photon scattering vector. For the Compton profiles of electrons in Si and O atoms we use the values of Biggs *et al.*[9] The Compton scattering cross-section of each shell has a value of zero in the energy region of the energy transfer, $E_0 - E$, smaller than the binding energy of an electron in the shell.

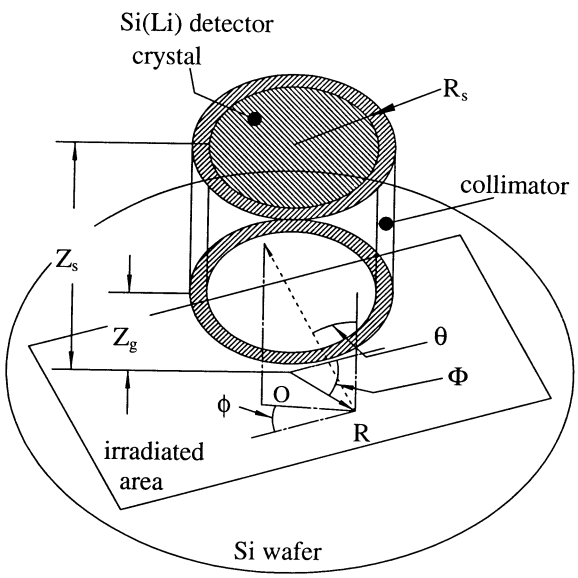

Figure 1. Geometry used to calculate the background spectra in SR-TXRF analysis. O is at the center of the detector system projected on the Si wafer. Polar coordinates (R, Φ) represent the point where fluorescence takes place. The polar angle, θ, and the azimuth angle, ϕ, represent the direction of fluorescence radiation from this point (R, Φ). R_s, Z_s and Z_g are the radius of the detector, the normal distance of the detector and the distance of the collimator from the wafer surface, respectively.

EXPERIMENTAL

The synchrotron radiation source used in this study was the beamline 10.3.2 of the Advanced Light Source at Lawrence Berkeley National Laboratory. The beam was focused horizontally by a spherical mirror and monochromatized by a double multilayer monochromator of W/B_4C. The beam size obtained was 6(V) × 0.06(H) mm^2 FWHM. The energy of the monochromator was set to 10.9 keV and the energy width of the multilayer optics was 200 eV. In addition to the primary reflection, the second harmonic was observed and its intensity was 2% of the first-order x-ray flux. Other higher order harmonics were suppressed by the cut-off mirror because the cut-off energy was approximately 22 keV.

It is important to determine accurately the incident flux for calculating absolute counts. The method used was to pulse count photons directly using a scintillator–PM tube combination, using a thick attenuator to reduce the intensity into the detector. Knowing the thickness and the absorption coefficient of attenuator, we can measure I_0. To make the measurement accurate, data were collected over a range of thickness. The greatest source of error of this method comes from the higher order Bragg peaks given by the multilayer monochromator. If we increase the absorber thickness the flux will be dominated by high-order light and the determination of flux will rapidly become incorrect. In this case we are fortunate that the Mo K edge suppresses the transmission at the second-order energy. We used eight pieces of Mo foil of 25 μm thickness. The foil thickness was selected for reducing errors due to higher order Bragg peaks

to <2%. The flux of the incident beam on the Si wafer was measured to be 2×10^9 photons s^{-1}.

An Si(Li) solid-state detector with an intrinsic resolution of 140 eV at Mn Kα was used. The radius of the detecting crystal was 1.5 mm and the thickness was 3 mm. A collimator of length 12 mm was attached in front of the detector to reduce the scattering intensity. As the collimator having a 1.5 mm radius was extended to detecting crystal, the effective dimensions of the Si crystal could be well defined. A 12.5 μm thick BN filter in front of the detector effectively attenuates the Si fluorescence x-rays to the detector. Data were collected with a 2 mm space between the filter and the wafer surface and the Be window was located 5.5 mm from the wafer surface.

In order to compare the calculated background spectrum with experimental results, spectra of a clean wafer were collected at various glancing angles. The critical angle is at 2.87 mrad for an incident x-ray of 10.9 keV. For each incident angle the measurements were repeated four times and the results were averaged. In the measured spectra, fluorescence signals from the impurities of Cl and Cu were present.

RESULTS AND DISCUSSION

The total Compton scattered counts were calculated by using Eqns (1) and (2) and the x-ray intensity distribution in the SiO_2 layer and Si wafer was computed by using the transfer matrix.[10] Figure 2 shows the variation of total Compton scattered counts as a function of glancing angle and SiO_2 layer thickness. The total Compton scattered count increases as the SiO_2 layer becomes thicker and the curves show peaks around the critical angle. The variation of Compton scattered count arises mainly from the increment of the penetration depth due to the SiO_2 layer on the Si wafer. The SiO_2 layer also influences the reflectivity, R, and the penetration depth, resulting in the variation of the photoelectron bremsstrahlung count. Figure 3 shows the variation of total photoelectron bremsstrahlung counts simulated by the Monte Carlo method.[6] The photoelectron bremsstrahlung count decreases as the SiO_2 layer becomes thicker and does not change much above the critical angle.

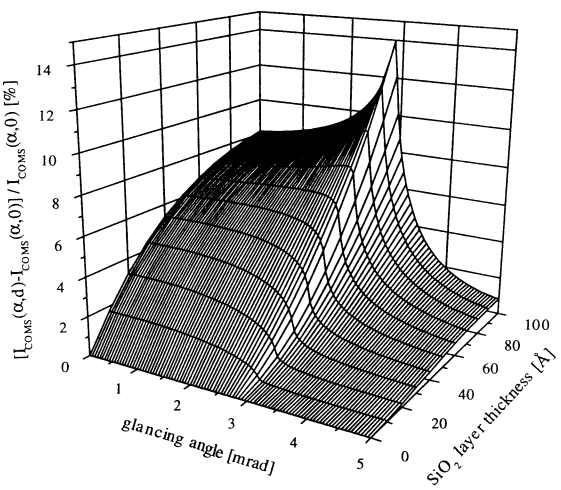

Figure 2. Variation in the Compton scattered counts, $[I_{COMS}(\alpha, d) - I_{COMS}(\alpha, 0)]/I_{COMS}(\alpha, 0)(\%)$, as a function of glancing angle, α, and SiO_2 layer thickness, d.

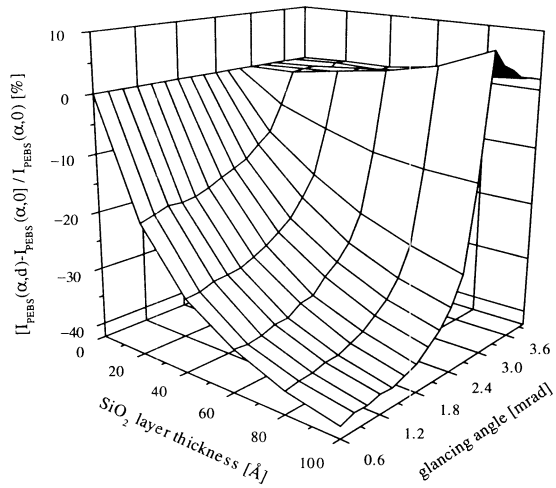

Figure 3. Variation in the photoelectron bremsstrahlung counts, $[I_{PEBS}(\alpha, d) - I_{PEBS}(\alpha, 0)]/I_{PEBS}(\alpha, 0)(\%)$, as a function of glancing angle, α, and SiO_2 layer thickness, d.

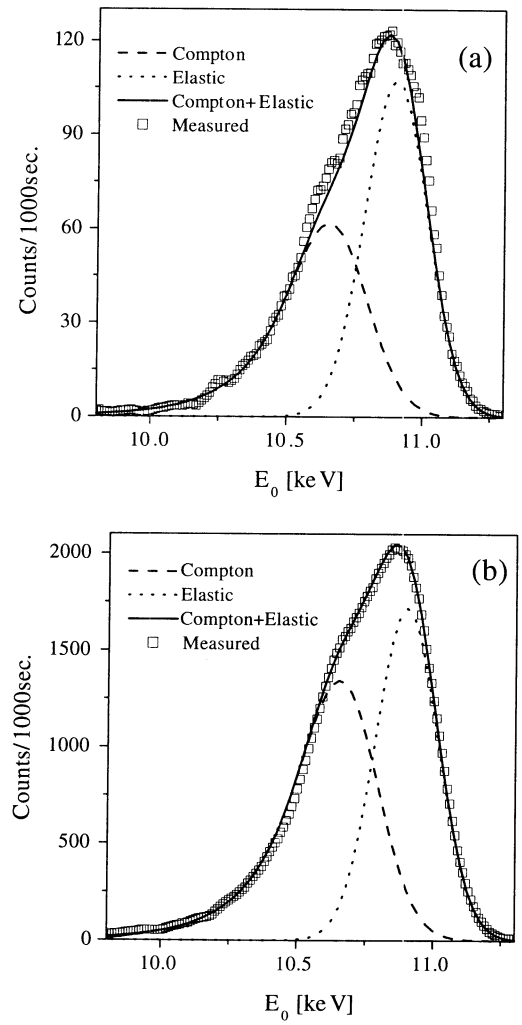

Figure 4. Comparisons of the calculated scattered spectra (Compton contribution = dashed line) and measured data (open squares) at glancing angles of (a) 2.2 and (b) 3.0 mrad.

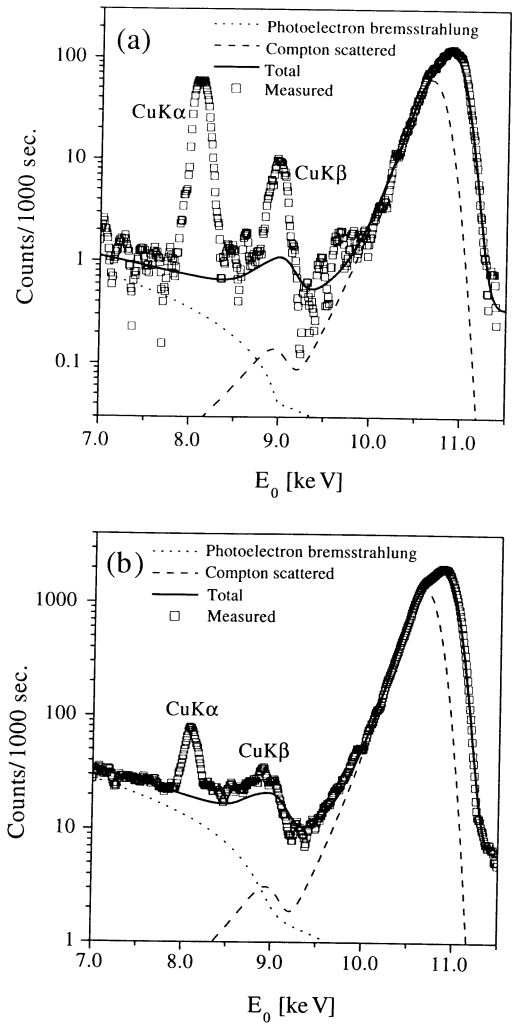

Figure 5. Detailed views of the calculated spectrum and the measured spectrum in the energy range where photoelectron bremsstrahlung and Compton scattering co-exist. The glancing angle is (a) 2.2 and (b) 3.0 mrad.

Because the photoelectron bremsstrahlung count is directly proportional to the number of photons absorbed in the wafer, Fig. 3 is similar to the transmissivity, $1 - R$, variation except for minor variations due to the change of the penetration depth.

By comparing the measured SR-TXRF spectra with the calculated ones at various thicknesses of the SiO_2 layer, the calculated background spectra assuming an SiO_2 layer of 15 Å thickness show good agreement. Figure 4 shows the comparison between the calculated Compton scattered spectra and measured data at incident angles of 2.2 and 3.0 mrad. The elastic scattered count, as shown in Fig. 4, is fitted as a Gaussian distribution to the measured data and does not contribute to the background spectrum. Figure 4 indicates that Compton scattering contributes mainly to the SR-TXRF background above 9 keV when the incident x-ray energy of 10.9 keV is used. In a lower energy range the Compton scattering and photoelectron bremsstrahlung spectrum co-exist as shown in Fig. 5. The total spectrum (solid line) in Fig. 5, which includes the Compton scattered count, the photoelectron bremsstrahlung count and the

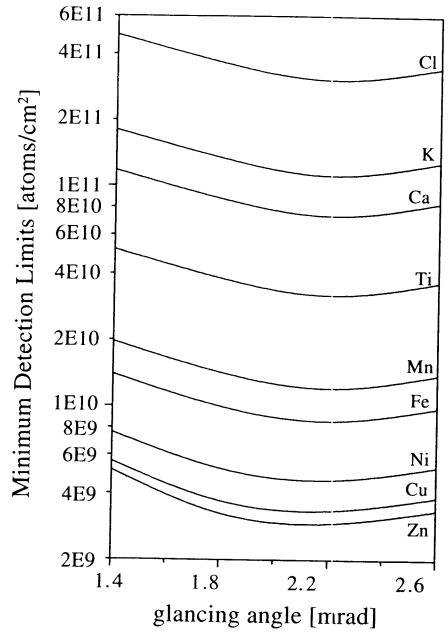

Figure 6. Theoretical detection limits of surface contaminants for SR-TXRF analysis of Si wafer as a function of the glancing angle. The values are calculated for an SiO_2 layer thickness of 15 Å and incident flux of 2×10^9 photons s^{-1}.

escaped peak from Si(Li) detector, shows good agreement with the measured spectrum. The peak around 9.1 keV in the background spectrum is formed by the escaping phenomenon (peak at 9.16 keV) and the K edge in the Compton profile of an Si atom (peak at 9.06 keV).

The fluorescence counts from contaminants near the surface of Si wafers within a few atomic layers are given by[10]

$$I_f = I_0[1 - R(\alpha)]\frac{\alpha}{\mathrm{Re}[\alpha_s]}\rho_s \tau P_K \omega_K g_{K\alpha} \pi R_{eff}^2 \frac{\Omega_{avg}}{4\pi}\eta \exp(-\mu_f t_f) \quad (3)$$

where $R(\alpha)$ is the reflectivity at the incident glancing angle α, α_s is the refraction angle of the Si wafer, ρ_s is the surface density and τ is the mass photoelectric absorption coefficient. P_K, ω_K and $g_{K\alpha}$ are the absorption jump factor of the K series, the fluorescence yield of the K series and the emission probability of the Kα line, respectively. πR_{eff}^2 is the area of the wafer as seen by the detector through the collimator in front of the detector and Ω_{avg} is the average solid angle of the detector seen from the wafer area, πR_{eff}^2. η is the detection efficiency of the Si(Li) detector, μ_f is the total attenuation coefficient of the filter and t_f is the thickness of the filter. With $Z_s = 14$ mm, $Z_g = 2$ mm and $R_s = 1.5$ mm, the average solid angle, Ω_{avg}, is calculated to be 27.0 msrad.

From the calculated background spectrum and fluorescence count, we can evaluate the MDL under given experimental conditions. Here, the background counts were calculated in the energy range of twice the fluorescence peak's FWHM. The FWHM values of fluorescence peaks were determined with electric noise of 48 eV and a Fano factor of 0.14; 98.1% of the fluorescence peak is within this width. As shown in Fig. 6, the calculated MDLs depend on the glancing angle. The glancing angle at which the lowest MDL value can be achieved does not

vary with the kind of element, and is around 2.2 mrad. In the case of Fe, for instance, the theoretical MDL of 8.59×10^9 atoms cm^{-2} is achieved at a glancing angle of 2.21 mrad.

CONCLUSION

When we know the concentration and the exact depth distribution of contaminants in a wafer, we can measure the MDLs of the contaminants by inspection of the wafer. However, it is not easy to measure the concentration and the exact depth distribution of ultra-trace contaminants. Therefore, the optimization of the experimental conditions by a theoretical approach is more practical. In this study, the background spectrum of SR-TXRF was quantitatively calculated from the composed counts of photoelectron bremsstrahlung and Compton scattered x-rays with respect to the SiO_2 layer on Si wafers. The theoretical MDLs in the SR-TXRF determination of contaminants on an Si wafer under given experimental conditions were determined.

Acknowledgments

The authors thank P. Pianetta of SSRL for assisting with the equipment for the SR-TXRF measurements and D. E. Kim of PAL for his support in computation.

REFERENCES

1. Comin F, Navizet M, Mangiagalli P, Apostolo G. *Nucl. Instrum. Methods B* 1999; **50**: 538.
2. Ortega L, Comin F, Formoso V, Stierle A. *J. Synchrotron Radiat.* 1998; **5**: 1064.
3. Mori Y, Kubota K, Shimanoe K, Sakon T. *Anal. Sci.* 1998; **14**: 275.
4. Wobrauschek P, Gorgl R, Kregsamer P, Streli Ch, Pahlke S, Fabry L, Haller M, Knochel A, Radtke M. *Spectrochim. Acta, part B* 1997; **52**: 901.
5. Pianetta P, Takaura N, Brennan S, Tomkins W, Laderman SS, Ficher-Colbrie A, Shimazaki A, Miyazaki K, Madden M, Wherry DC, Kortright JB. *Rev. Sci. Instrum.* 1995; **66**: 1293.
6. Shin NS, Chang CH, Koo YM, Padmore H. *J. Appl. Phys.* 1999; **86**: 902.
7. Ribberfors R. *Phys. Rev. A* 1983; **27**: 3061.
8. Namito Y, Ban S, Hirayama H. *Phys. Rev. A* 1995; **51**: 3036.
9. Biggs F, Mendelsohn LB, Mann JB. *At. Data Nucl. Data Tables* 1975; **16**: 201.
10. Klockenkamper R. *Total-Reflection X-Ray Fluorescence Analysis.* Kohn Wiley: New York, 1997; 41–86.